energies

MDPI

Article

Study on the Design and Development of Advanced Inorganic Polymers for Thermal Energy Storage (TES) Systems

Ioanna Giannopoulou [1,*], Loizos Georgiou [2], Konstantina Oikonomopoulou [1], Maria Spanou [1,3], Alexandros Michaelides [2] and Demetris Nicolaides [1,3]

[1] Frederick Research Center, Nicosia 1035, Cyprus; oikonomopoulou.konstantina@ucy.ac.cy (K.O.); res.mas@frederick.ac.cy (M.S.); d.nicolaides@frederick.ac.cy (D.N.)
[2] RTD TALOS Ltd., Nicosia 2404, Cyprus; lg@talos-rtd.com (L.G.); am@talos-rtd.com (A.M.)
[3] Department of Civil Engineering, Frederick University, Nicosia 1036, Cyprus
* Correspondence: ionagian@outlook.com

Abstract: Thermal Energy Storage (TES) technologies improve solar power dispatchability by addressing the important challenge of energy intermittency. Sensible heat energy storage technology using materials based on Ordinary Portland Cement (OPC) is the simplest and most economical. However, the operation of these materials is limited to temperatures below 400 °C due to the structural degradation of OPC at this temperature. This paper investigates the design and development of inorganic polymers based on Construction and Demolition Waste (CDW) as a sustainable, low-cost, and environmentally friendly alternative to OPC-based materials for high-temperature sensible TES applications. Based on the ternary systems Na_2O-SiO_2-Al_2O_3 and K_2O-SiO_2-Al_2O_3, representative compositions of CDW-based inorganic polymers were theoretically designed and evaluated using the thermochemical software FactSage 7.0. The experimental verification of the theoretically designed inorganic polymers confirmed that they can withstand temperatures higher than 500 and up to 700 °C. The optimized materials developed compressive strength around 20 MPa, which was improved with temperatures up to 500 °C and then decreased. Moreover, they presented thermal capacities from 600 to 1090 J kg^{-1} °C $^{-1}$, thermal diffusivity in the range of 4.7–5.6 × 10^{-7} m^2 s^{-1}, and thermal conductivity from 0.6 to 1 W m^{-1} °C^{-1}. These properties render the developed inorganic polymers significant candidates for TES applications.

Keywords: inorganic polymer; geopolymer; thermal energy storage; thermodynamics; ternary oxide system; elevated temperatures; structural stability; thermal conductivity

Academic Editors: Yuekuan Zhou, Zengguang Sui, Chong Zhai and Zhixiong Ding

Received: 29 April 2025
Revised: 26 May 2025
Accepted: 10 June 2025
Published: 12 June 2025

Citation: Giannopoulou, I.; Georgiou, L.; Oikonomopoulou, K.; Spanou, M.; Michaelides, A.; Nicolaides, D. Study on the Design and Development of Advanced Inorganic Polymers for Thermal Energy Storage (TES) Systems. *Energies* **2025**, *18*, 3107. https://doi.org/10.3390/en18123107

1. Introduction

Thermal Energy Storage (TES) systems are central to the global clean energy transition and reduction in greenhouse gas emissions, as heat energy counts today for almost 20% of the global energy consumption and more than 60% of the global industrial energy demand [1]. Since the vast majority of the industrial heat energy demand relies on fossil fuels, it also contributes to most of the global-energy-related CO_2 emissions. This contribution was predicted to reach 25% in 2024 [1]. Nowadays, the share of renewables in heat energy demand is very small and limited to industrial sectors with low-temperature requirements, such as the food industry. The most significant challenges that renewable energy has to face in order to increase its share in heat energy are related to the intermittent nature of renewable sources and the wide variety of temperature levels for processes and end-uses in the different industrial sectors. In this context, TES systems are essential to improve the

efficiency and dispatchability of renewable energy plants, especially those of solar power that are predominant in thermal energy production.

TES systems are based on different types of materials, including crystalline and amorphous solid materials, as well as liquids, which can be classified into three categories: sensible, latent, and thermochemical heat storage materials [2]. Among the materials of the first category, natural rocks, Ordinary Portland Cement (OPC)-based materials, ceramics, and molten salts are the most commonly used and researched [3–5]. The TES materials of the second category that are mostly used include organic, inorganic, and eutectic Phase Change Materials (PCMs) [6–9]. The thermochemical TES materials emerged during recent decades, relying on a reversible process that involves adsorption, chemical reactions, and resorption. For low-temperature applications, solid and liquid adsorbents based on zeolites and various solutions [6,10], as well as the innovative Metal Organic Frames (MOFs), are common, while for high-temperature applications, specific systems of metal hydroxides, carbonates, and hydrates [11] are investigated.

Sensible heat storage is the simplest and most economical technology to store thermal energy. For applications in temperatures up to 200 °C, cost-effective materials, such as water, natural rocks, and ceramics, are commonly used [2]. For high-temperature applications above 200 °C, molten salts, rocks, ceramics, and cementitious materials based on OPC can be used [12]. The structural integrity of the TES materials at high temperatures is a major challenge for their viability. Due to the thermal stability at elevated temperatures, solid materials are preferred for temperatures between 300 and 400 °C, in contrast to molten salts and other organic liquids, which exhibit an increased risk of decomposition, breakdown, leakage, or spillage. At this temperature range, concrete is an ideal energy storage solution, as it has easy handling and low cost, while it is based on raw materials that are abundant and available everywhere. In recent years, the research on new types of cement and specialized compositions of concrete yielded notable progress, achieving cement-based materials for TES applications up to the temperature of 550 °C [13–15]. However, the limitations of cement concrete at such high temperatures have prompted research into alternatives, such as geopolymer concrete [16]. Furthermore, the increasing operation of Concentrated Solar Power (CSP) plants and the adoption of Solar Process Heat (SPH) and Industrial Waste Heat (IWH) processes has led the research interest towards materials with high-temperature tolerance, higher than 600 °C, in order to be used in these applications.

Inorganic polymers or geopolymers are promising alternatives to OPC-based materials for high-temperature TES applications due to the low environmental footprint of their production process, the high compressive strength and durability, and the good thermophysical properties. The inorganic polymers are formed through the alkali activation of various, mostly secondary, solid sources of aluminosilicate composition, such as metallurgical slags, fly ash, waste glass, construction and demolition waste, and other industrial waste and residues, which contain reactive aluminosilicate phases. The resulting materials present unique mechanical and thermophysical properties, durability, corrosion resistance in extreme environments, fire resistance, and non-combustibility [16,17]. In contrast to concrete, which suffers severe spalling when exposed to temperatures between 300 and 450 °C [18], even though it is also a non-combustible material with inherent fire resistance, the geopolymers (inorganic polymers) maintain their structural stability and mechanical properties at the temperatures between 600 and 800 °C [19–21], while their compressive strength lies after cooling down [20,21]. Particularly, the inorganic polymers based on the brick waste of CDW behaved as elastic materials up to the temperature of 950 °C [20] and maintained their compressive strength close to its initial value. Geopolymers have the ability to remain stable at high temperatures due to their specific microstructure, which is affected by the silicon-to-aluminum (Si/Al) molar ratio [21,22] that determines the type

and the extent of the crystalline phases formed in the geopolymer matrix at high temperatures. Moreover, the thermal deformation of geopolymers at elevated temperatures, as well as their mechanical and thermal properties, depend on the type and total concentration of alkali in the geopolymer system [19,22]. The suitability of inorganic polymers for high-temperature applications compared to OPC concrete is related to the different microstructural evolution during heating, which affects critical properties of the materials, such as strength retention, thermal expansion, thermal conductivity, and microstructural porosity [23,24]. In contrast to OPC, in which water is an integral part of the contained calcium silicate hydrate (C-S-H) phases, inorganic polymers contain a small portion of physically and chemically bonded water in their matrix. During heating, the reactions of the geopolymer matrix dehydration and dehydroxylation take place in the range of 100–300 °C and at slightly raised temperatures than 300 °C, respectively. At about 600 °C, the geopolymer matrix densifies due to the sintering phenomenon [23] that improves the inter-particle connection, resulting in less porous microstructures and, thus, becomes more durable. As the temperature rises to about 800 °C, the crystallization of the amorphous geopolymer matrix occurs, resulting in ceramic-like materials with relevant properties [25]. By contrast, when OPC is exposed to elevated temperatures, the dehydration of the C-S-H gel phase takes place between 200 and 355 °C [26], and the dissociation of portlandite, $Ca(OH)_2$, to calcium oxide (CaO) between 515 and 615 °C [26]. Both these reactions result in volume expansion of the OPC matrix that damages structural integrity. After cooling down, cement gradually rehydrates by reabsorbing moisture from the environment. However, the amount of water reabsorbed in cement remains lower than the initial state before its exposure to high temperatures. In addition to the superiority of inorganic polymers over OPC in terms of thermal stability and structural integrity at high temperatures, it is worth pointing out that the production of inorganic polymers utilizes solid wastes and reduces the CO_2 emissions of OPC production process by 40–60% [23].

The main field of inorganic polymer high-temperature applications concerns the passive fire protection of buildings and constructions, as these materials can withstand temperatures higher than 1000 °C [27–29]. However, according to recent studies, inorganic polymer binders have been used in foundry works and combustion linings and tooling [30,31], presenting excellent thermo-mechanical performance. Moreover, the partial or full replacement of calcium aluminate cement used in high-alumina refractories by geopolymers was investigated [32]. The developed materials presented a remarkable performance at high temperatures and improved ceramic densification due to the synergies of the raw solid materials towards the reduction in cement hydration and the enhancement of the geopolymerization processes.

In the field of TES applications, there are few research publications regarding the utilization of inorganic polymers or geopolymers. Specifically, a geopolymer hybrid cement, which contained 20% of OPC and 80% inorganic polymers, was tested at temperatures higher than 500 °C, and its thermal behavior and properties were experimentally measured and theoretically predicted through numerical modeling [33–35]. The addition of carbon or nickel fibers in a geopolymer cement developed for sensible TES applications improved its thermophysical properties and accelerated the charging/discharging process, considering the environmental effects [36].

The present research work is motivated by a need to develop simple and sustainable materials for TES applications that can operate at temperatures above 400 °C, in which competitive OPC-based materials are subjected to severe structural degradation. Inorganic polymers (geopolymers) are advanced, low-cost, and sustainable materials for effective and feasible, technologically and economically, renewable energy storage. These materials can withstand elevated temperatures by maintaining their structural stability and integrity.

Moreover, they can provide sustainability in the energy storage sector and contribute to the reduction in the environmental footprint, as they are based on secondary raw materials and use a technology with low energy requirements and CO_2 emissions.

In this paper, a comprehensive theoretical approach that can lead to the proper formulations of inorganic polymers, which are based on Construction and Demolition Waste (CDW), is developed. Based on the ternary oxide systems of (Na_2O/K_2O)-SiO_2-Al_2O_3, which correspond to the critical components of the inorganic polymers, and specific thermodynamic software, different formulations of the CDW-based inorganic polymers that can withstand temperatures up to 750 °C were theoretically designed. The findings of the theoretical investigation were evaluated through a series of experiments, focusing on the development of CDW-based inorganic polymers for thermal energy storage applications at temperatures up to 750 °C. The resulting materials were tested in terms of mechanical and thermal properties, while their microstructure was evaluated according to specific instrumental methods.

2. Theoretical Synthesis of Thermal Energy Storage Inorganic Polymers

The critical function of a Thermal Energy Storage (TES) material is to store surplus energy in the form of heat during high production periods and release it, either as heat or electricity, during periods of high demand. The ability of a material to operate as a heat store is related to its thermal conductivity and endothermicity. Moreover, the structural stability and integrity of a material at high temperatures allow it to operate at elevated temperatures without deforming or degradation, thus enhancing its storage capacity. A material can withstand an elevated temperature if its composition has a solidus temperature above and a melting point significantly higher than this temperature. The phase diagrams of the ternary oxide systems Na_2O-SiO_2-Al_2O_3 and K_2O-SiO_2-Al_2O_3, which represent the most significant components of inorganic polymers (geopolymers), can predict theoretically materials with structural stability and integrity at elevated temperatures. Considering the phase diagrams of these oxide ternary systems, CDW-based inorganic polymers with structural stability up to 750 °C were theoretically formulated and evaluated through thermodynamic calculations of equilibrium compositions using the FactSage 7.0 software. The theoretical approach of inorganic polymer composition design was based on the following methodology. Initially, several compositions located in stability areas of the ternary Na_2O-SiO_2-Al_2O_3 or K_2O-SiO_2-Al_2O_3 phases diagram that have liquidus temperatures above 700 °C were considered to represent totally dehydrated inorganic polymers derived from the geopolymerization of the brick waste (WB) used as a solid precursor in this work with alkali (sodium or potassium) hydroxide solutions. In certain cases, the doping of the geopolymer system with aluminum or silicon oxide was also considered. Subsequently, the thermal stability of the selected inorganic polymer compositions at elevated temperatures was theoretically evaluated through the calculation of their solidus temperature. Finally, the mechanical and thermophysical properties of the theoretically designed inorganic polymers for TES applications were experimentally verified. In Figure 1, the projection of the liquidus surface in the ternary system Na_2O-SiO_2-Al_2O_3 at one atm [37] is shown. The points marked P1 to P9 in this phase diagram (Figure 1) concern fully dehydrated inorganic polymer compositions considered for theoretical study in this research. All points were located in the stability areas of albite ($Na_2O{\cdot}Al_2O_3{\cdot}6SiO_2$) that melts at 1118 °C and nepheline ($Na_2O{\cdot}Al_2O_3{\cdot}2SiO_2$) with melting point at 1256 °C. According to the ternary Na_2O-SiO_2-Al_2O_3 phase diagram (Figure 1), the materials included in the albite area have liquidus temperatures between 732 and 1108 °C, while the liquidus temperatures of those materials included in the area of nepheline range from 768 to 1280 °C. Therefore, the inorganic polymers corresponding to the compositions selected for this theoretical analysis are

expected to remain structurally stable at temperatures up to 700 °C. In the phase diagram shown in Figure 1, the point marked P0 indicates the chemical composition of WB raw material used in this research, considering that it consists only of the ternary Na_2O-SiO_2-Al_2O_3 system's oxides. The normalized composition of WB contained 78.22 wt% SiO_2, 20.01 wt% Al_2O_3, and 1.60 wt% Na_2O with molar ratios of SiO_2 to Al_2O_3 and Na_2O to SiO_2 equal to 6.54 and 0.02, respectively. The inorganic polymer compositions P1 to P9 shown in Figure 1 form three groups, depending on their molar ratios Na_2O/Si_2O and SiO_2/Al_2O_3 (Table 1). In particular, the compositions marked P1 to P5 in the Na_2O-SiO_2-Al_2O_3 phase diagram (Figure 1) lie on a line connecting point P0 (composition of WB) to the Na_2O edge of this diagram and correspond to fully dehydrated inorganic polymers derived through the geopolymerization of the WB raw material with sodium hydroxide (NaOH) solutions of decreasing concentration. Therefore, the fully dehydrated inorganic polymers with compositions at points P1 through P5 have similar SiO_2/Al_2O_3 molar ratios, which are also almost similar to that of the WB raw material, and decreasing Na_2O/SiO_2 molar ratios (Table 1).

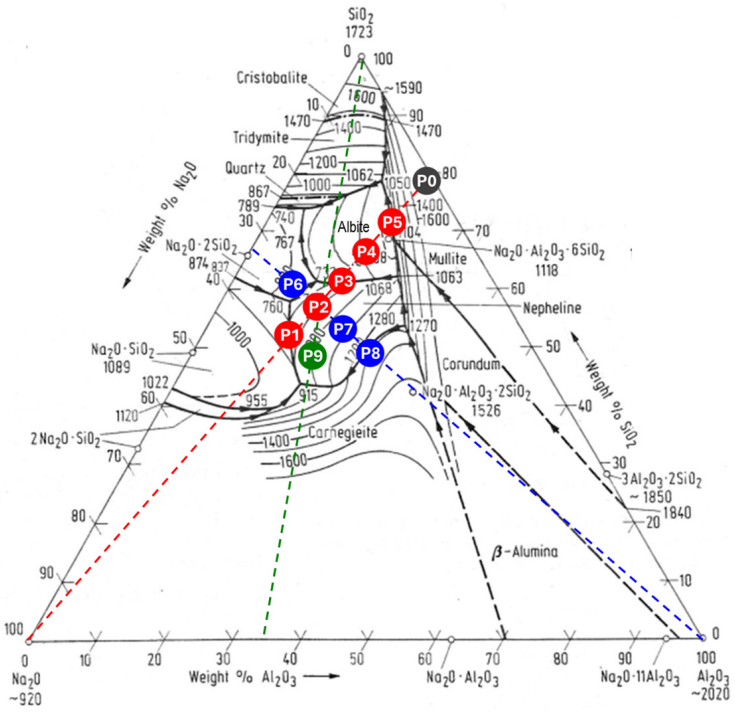

Figure 1. Liquidus temperature surface in the Na_2O-SiO_2-Al_2O_3 ternary system [37] and placement of the investigated Na-based inorganic polymer compositions (fully dehydrated).

Table 1. Inorganic polymer compositions selected in the ternary oxide system Na_2O-SiO_2-Al_2O_3.

Oxides	P(1)	P(2)	P(3)	P(4)	P(5)	P(6)	P(7)	P(8)	P(9)
					Mass Fraction (wt%)				
SiO_2	51.16	56.50	61.79	65.16	73.17	60.84	52.38	49.65	50.23
Al_2O_3	14.23	15.75	17.25	18.72	20.21	9.70	21.49	25.62	18.63
Na_2O	34.60	27.76	20.97	16.12	6.62	29.47	26.13	24.73	31.14
Total	100	100	100	100	100	100	100	100	100
Molar Ratios					Mole Fraction (mole/mole)				
SiO_2/Al_2O_3	6.11	6.10	6.09	5.92	6.15	10.67	4.14	3.29	4.58
Na_2O/SiO_2	0.65	0.48	0.33	0.24	0.09	0.47	0.48	0.48	0.60

Similarly, the compositions P6, P2, P7, and P8 in the Na_2O-SiO_2-Al_2O_3 phase diagram (Figure 1) align along a line connecting point P2 and the Al_2O_3 edge of this diagram and imply totally dehydrated inorganic polymers, which have similar Na_2O/SiO_2 molar ratios and decreasing SiO_2/Al_2O_3 molar ratios (Table 1). Finally, the compositions denoted by P2 and P9 in the Na_2O-SiO_2-Al_2O_3 phase diagram (Figure 1) are located on a line that connects the SiO_2 edge of this diagram to point P2. The compositions P2 and P9 represent totally dehydrated inorganic polymers with quite similar molar ratios of Na_2O/SiO_2 and decreasing SiO_2/Al_2O_3 molar ratios (Table 1).

In order to evaluate the findings of the theoretical analysis performed to formulate thermal energy storage inorganic polymers, the solidus temperatures of the inorganic polymers' compositions indicated by points P1 to P9 in the phase diagram given in Figure 1 were identified through thermodynamic calculations, using the software FactSage 7.0. Based on this software, the portion of each material that was melted between solidus and liquidus temperatures was also calculated. For all these thermodynamic calculations, the module "Equilib" and the databases FToxide (oxide database for multiple elements) and FactPS (pure substances database containing compounds and phases) of the software FactSage 7.0 were employed. Specifically, considering that each inorganic polymer composition marked P1 to P9 in the phase diagram of Figure 1 is in the form of chemical oxides, the module "Equilib" predicted the portion and composition of liquid and solid phases formed at equilibrium at various temperatures. The liquid and solid phases were identified for each inorganic polymer composition in a temperature range from 500 to 1500 °C with a step of 50 °C. The results are presented in Figure 2.

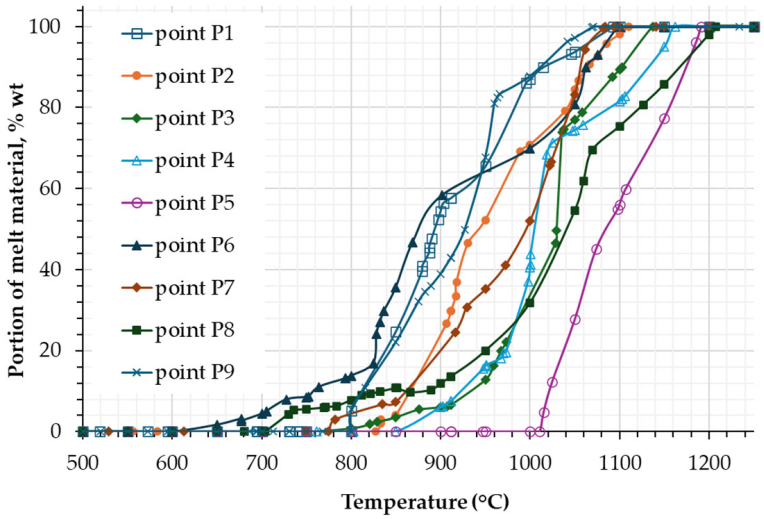

Figure 2. Portion of melt (wt%) between solidus and liquidus temperatures of the fully dehydrated inorganic polymer compositions P1–P9, versus temperature.

According to Figure 2, the solidus temperatures of inorganic polymer compositions P6 and P8 listed in Figure 1 were below and slightly above, respectively, the temperature of 700 °C. Although the percentage of melt for both these concentrations at the temperature of 750 °C was below 10% (Figure 2), they were excluded from further investigation in this work. As seen in Table 1, these compositions refer to the highest and lowest SiO_2/Al_2O_3 molar ratios among the investigated ones, both of which are contraindicated for the production of inorganic polymers (geopolymers). Low molar ratios of SiO_2/Al_2O_3 (<3.5) combined with Na_2O/Al_2O_3 molar ratios higher than 1.0 enhance the formation of crystalline zeolites (faujasite and zeolite A), rather than the X-ray amorphous geopolymeric phase, resulting in low strength materials [38–40]. At molar ratios of SiO_2/Al_2O_3 higher than 6.0 and of Na_2O/Al_2O_3 higher than 1.5, sodium bicarbonate compounds are formed

within the geopolymeric structures, reducing the compressive strength of the obtained materials [39,40].

As shown in Figure 2, all the other inorganic polymer compositions listed in Figure 1 presented solidus temperatures above 750 °C, and, therefore, they were selected in this work to be experimentally studied for the development of WB-based inorganic polymers for thermal energy storage.

In Figure 3, the projection of liquidus temperatures in the ternary oxide system K_2O-SiO_2-Al_2O_3 at one atm [37] is shown. In the phase diagram illustrated in Figure 3, the area of leucite ($K_2O{\cdot}Al_2O_3{\cdot}4SiO_2$) with a melting point at 1693 °C is the most suitable for the formulation of WB-based TES inorganic polymers that will maintain their structural stability at temperatures up to 750 °C. According to Figure 3, the material compositions located in the leucite area present liquidus temperatures between 1000 and 1600 °C, while those located in the neighboring region of potassium feldspars ($K_2O{\cdot}Al_2O_3{\cdot}6SiO_2$) have liquidus temperatures ranging from 695 to 867 °C. Therefore, the compositions of inorganic polymers located in the leucite region are expected to remain 100% solidified at elevated temperatures up to 750 °C.

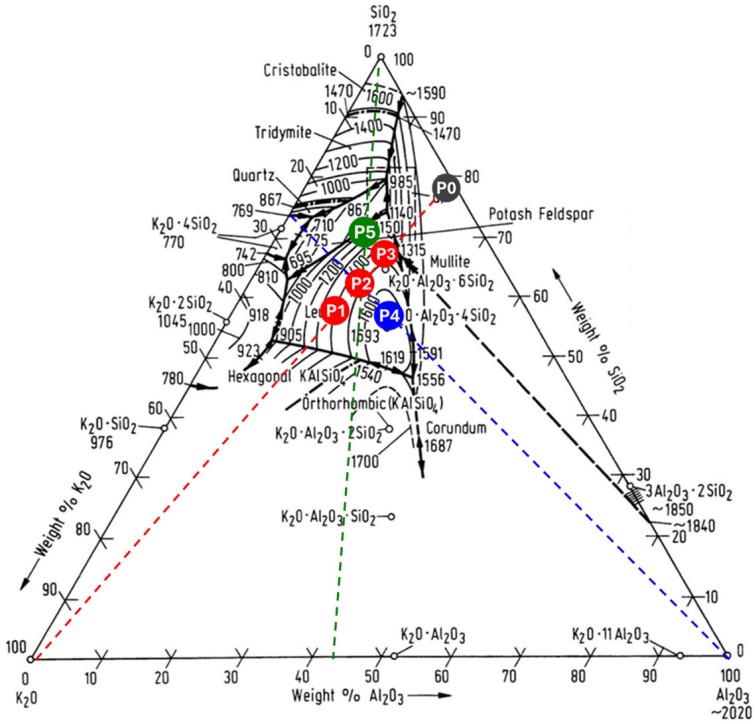

Figure 3. Liquidus temperature surface in the K_2O-SiO_2-Al_2O_3 ternary system [37] and placement of the investigated inorganic polymer compositions (fully dehydrated).

For the theoretical analysis of TES inorganic polymers in the ternary oxide K_2O-SiO_2-Al_2O_3 system, the fully dehydrated inorganic polymer compositions marked P1 to P5 in the phase diagram given in Figure 3 were selected. Point P0, also marked in this phase diagram, indicates the chemical composition of the WB raw material used in this study after normalization according to the oxides of the relevant ternary system. The normalized composition of WB consists of 76.70 wt% SiO_2, 19.63 wt% Al_2O_3, and 3.68 wt% K_2O, with mole fractions (mole/mole) SiO_2 to Al_2O_3 to K_2O equal to 0.85 to 1.13 to 0.03. The mass fraction of the selected inorganic polymer compositions, along with the molar ratios Na_2O/Si_2O and SiO_2/Al_2O_3, are summarized in Table 2.

Table 2. Inorganic polymer compositions selected in the ternary oxide system K_2O-SiO_2-Al_2O_3.

Oxides	P(1)	P(2)	P(3)	P(4)	P(5)
			Mass Fraction (wt%)		
SiO_2	57.27	61.99	67.09	57.22	57.26
Al_2O_3	15.13	16.04	17.15	23.14	20.68
K_2O	27.60	21.97	15.77	19.64	22.06
Total	100	100	100	100	100
Molar Ratios			Mole Fraction (mole/mole)		
SiO_2/Al_2O_3	6.44	6.57	6.65	4.20	4.11
K_2O/SiO_2	0.31	0.23	0.15	0.22	0.25

As shown in Figure 3, the compositions at points P1 to P3 in the K_2O-SiO_2-Al_2O_3 phase diagram correspond to fully dehydrated inorganic polymers produced through the geopolymerization of the WB raw material with potassium hydroxide (KOH) solutions of decreasing concentration. According to Table 2, these compositions have a decreasing K_2O/SiO_2 molar ratio and an almost similar SiO_2/Al_2O_3 molar ratio, which is also close to the one of the raw material WB. The other two compositions, marked P4 and P5 in the phase diagram given in Figure 3, lie on the lines connecting point P2 of the phase diagram and its edges Al_2O_3 and SiO_2, respectively. Compared to the composition at point P2, these inorganic polymer compositions have almost similar K_2O/SiO_2 molar ratios and decreasing SiO_2/Al_2O_3 molar ratios (Table 2). The equilibrium calculations performed for all inorganic polymer compositions located in the K_2O-SiO_2-Al_2O_3 phase diagram (Figure 3) revealed that their solidus temperature was higher than 900 °C. Therefore, all these compositions were selected for the development of WB-based geopolymers in this work.

3. Materials and Methods

3.1. Starting Materials and Chemicals

Table 3 summarizes the chemical analysis of the solid raw materials used in this research study for the development of WB-based thermal energy storage inorganic polymers (TES-IP). Specifically, two brick waste samples with similar chemical compositions and metakaolin were used. The first brick waste sample, WB-1, was delivered from a recycling plant of construction and demolition waste in Cyprus [20], while the second one, WB-2, was the scrap produced by a company that produces bricks and roof tiles in Cyprus. The sample of metakaolin (MK) was provided by the company IMERYS INDUSTRIAL MINERALS GREECE S.A (Kifisia, Greece). The chemical analysis of these samples was performed using the X-ray fluorescence (XRF) method and a SPECTRO Xepos ED-XRF spectrometer (SPECTRO Analytical Instruments AMETEK, Kleve, Germany). The concentrations of the oxides given in Table 3 are the average of four analyses carried out for each raw material.

According to Table 3, both the brick waste samples (WB-1 and WB-2) are rich in silicon oxide and aluminum oxide, having almost similar concentrations in both oxides. They also contain increased amounts of calcium oxide and iron oxide, with WB-1 having a higher iron oxide content and WB-2 having an increasing concentration of calcium oxide. Metakaolin (MK) consists almost entirely of silica and alumina.

Table 3. Chemical composition (oxide basis) of the raw materials used in this research.

Oxides	WB-1	WB-2	MK
		Mass, wt%	
SiO_2	53.57	51.20	43.48
Al_2O_3	14.33	12.48	53.94
CaO	7.71	13.15	0.05
FeO	10.19	7.95	0.54
K_2O	3.74	1.28	0.12
MgO	4.07	5.58	0.39
Na_2O	0.66	1.71	0.11
TiO_2	1.46	0.72	1.41
Other	4.27	5.93	-
Total	100.00	100.00	100.00

The mineralogical analysis of the used raw materials was performed through the X-ray diffraction (XRD) method on a D8 Bruckner diffractometer, using Cu K radiation (λ = 15,418 Å) operating at 40 kV, 30 mA at the 2θ range from 5° to 70° with a 0.02° s^{-1} scanning step. According to this analysis, both brick waste samples WB-1 and WB-2 consisted primarily of quartz (SiO_2) and feldspars (albite, $NaAlSi_3O_8$, and anorthite, $CaAl_2Si_2O_8$) and secondarily of calcite ($CaCO_3$) and hematite (Fe_2O_3). Traces of diopside ($MgCaSi_2O_6$) and mullite ($Al_6Si_2O_{13}$) were also identified in both samples. The mineralogical analysis of metakaolin revealed that it consisted primarily of an amorphous silicate/aluminosilicate phase registered in 2θ range between 17° and 30° and, secondarily, of the crystalline phases of quartz (SiO_2), illite, $[K_{05}(Al, Fe, Mg)_3(Si, Al)_4O_{10}(OH)_2]$, and anatase ($TiO_2$).

Except for the solid raw materials (geopolymer precursors), aqueous solution of sodium hydroxide (NaOH) with 6 M (mol/L), 7 M, and 8 M concentrations, and of potassium hydroxide with 4 M, 5 M, and 6 M concentrations were also used for the development of TES-IP in this research. These solutions were prepared by dissolving NaOH or KOH anhydrous pellets of analytical grade (MERCK S.A., Athens, Greece, 99.5% purity) in distilled water. The solutions were prepared 24 h in advance. Moreover, a sodium silicate aqueous solution of analytical grade provided by MERCK S.A. (Na_2O = 8%, SiO_2 = 27%, H_2O = 65% and d = 1.346 g/mL) and a potassium silicate aqueous solution of high purity (>99%) provided by the Greek manufacturing MULTIPLASS S.A., Athens, Greece (K_2O = 13%, SiO_2 = 27%, H_2O = 60% and d = 1.375 g/mL) were used for the preparation of the inorganic polymers.

3.2. Experimental Procedures

The inorganic polymers studied in this research were prepared by mixing the geopolymer precursor with the alkaline activating solution (mixture of hydroxide and silicate solutions of the same alkali) in a mechanical mixer at a speed of 750 rpm for 5 min to form a homogeneous and viscous paste. The obtained geopolymer paste was then cast in cubic silicon molds with sides of 35 mm. The formed specimens were cured at 70 °C for 48 h under atmospheric pressure. For the first 24 h, they were cured in the closed molds, while for the remaining 24 h, they were demolded and cured sealed with a plastic film, as this curing regime was proved optimum in previous research [41,42]. After curing, the specimens were stored for hardening at room temperature and dry conditions for 28 days before any measurement or analysis. This hardening period was considered adequate for CDW-based inorganic polymers to reach a high level of mechanical strength [20]. During the hardening procedure, the specimens were sealed with a plastic film to avoid the formation of alkali carbonates on their surface, which could affect their compressive strength.

To elucidate the thermal stability and structural integrity of the inorganic polymers developed in thermal energy storage applications, they were exposed at elevated temperatures of 300, 500, and 700 °C for 2 h, using a laboratory electric furnace (Figure 4a). In each testing temperature, two specimens of each material were put in the furnace, which operated at a heating rate of 4.4 °C/min to reach the predefined temperature. The specimens were left at this temperature for 2 h, and then the furnace was turned off, and the specimens were left in the furnace to cool down at an ambient temperature. In Figure 4b, the experimental procedure followed in these tests is illustrated.

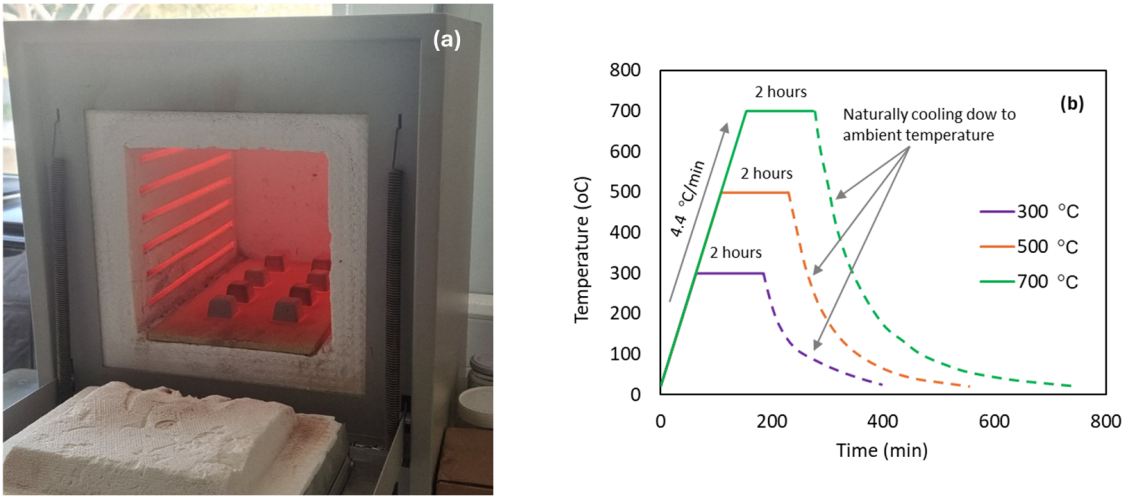

Figure 4. (**a**) Laboratory electric furnace used for testing the inorganic polymers at elevated temperatures; (**b**) experimental procedure followed in the thermal testing.

After cooling down, the specimens were visually inspected for cracks and signs of deformation and spalling and then tested for compressive strength. Their density and mass loss at each testing temperature were also determined. Furthermore, the structural rearrangements that occurred in their matrix were evaluated according to XRD analysis.

3.3. Measurements and Analyses

The compressive strength measurements of the inorganic polymer samples were performed on a 2000 kN electro-hydraulic testing machine with mechanical loading. The cured samples were tested after 28 days of hardening, while those exposed to elevated temperatures were tested 24 h after cooling down to ambient temperature. The compressive strength stated for each material in this work is the average of three measurements performed using three different specimens of the material.

The density of the inorganic polymers was determined as the mass per unit volume ratio (Equation (1)), while the mass loss after exposure to elevated temperature is expressed as the percentage of mass reduction. The reported density and mass loss values are the average of three replicates.

$$\rho\ (g/cm^3) = m/V \quad (1)$$

where m (g) and V (cm^3) are the mass and apparent volume, respectively, of the inorganic polymer sample.

The specific heat capacity of the inorganic polymers was determined according to the differential scanning calorimetry (DSC) method, using a SETARAM Themys One instrument (SETARAM KEM Technologies, BEST BUY ANALYTICAL Ltd., Athens, Greece). Sample powders of inorganic polymers with grain sizes lower than 63 μm were used. The

experiments were performed on heating between 25 and 600 °C with a heating rate of 5 °C/min under an inert atmosphere (He gas).

The thermal diffusivity measurements were carried out using the Laser Flash Analysis (LFA) technique, using a NETZSCH LFA 427 Microflash Analyzer (ANALYTICAL INSTRUMENTS S.A., Athens, Greece). The inorganic polymer sample powders (grain size < 63 μm) were pressed on a manually operating hydraulic press, applying 5 tons for 3 min to form pellets with a diameter of 10 mm and thickness of ~2 mm. Measurements were carried out at 100, 300, 500, and 700 °C with a heating rate of 10 °C/min. Three laser shots were performed at each temperature, with an interval of 2 min between shots to allow homogenization of the sample temperature.

The thermal conductivity of the inorganic polymers was calculated through Equation (2).

$$\lambda\ (W/m{\cdot}K) = a{\cdot}\rho{\cdot}C_p \quad (2)$$

where a (m^2/s) is the thermal diffusivity, ρ (kg/m^3) is the density, and C_p (J/kg·K) is the specific heat capacity of the inorganic polymer sample.

4. Results and Discussion

4.1. Thermal Stability of Inorganic Polymers at Elevated Temperatures

Table 4 summarizes the synthesis conditions of the WB-based inorganic polymers selected in the Na_2O-SiO_2-Al_2O_3 ternary system, according to the thermodynamic studies, for experimental optimization regarding their suitability in thermal energy storage applications. Similarly, Table 5 summarizes the synthesis conditions of the WB-based inorganic polymers selected in the K_2O-SiO_2-Al_2O_3 ternary system for experimental optimization. The raw material sample WB-1 (Table 3) was used for the production of the Na-based inorganic polymers (Table 4), while the K-based inorganic polymers (Table 5) were produced using the raw material sample WB-2 (Table 3). Figure 5 illustrates the compressive strength measurements of all studied inorganic polymers.

Table 4. Synthesis conditions of sodium-based inorganic polymers.

IP Code Name	WB-1/MK (wt%)	[NaOH] (M)	S/L [1] (g/mL)	Molar Ratios		$NaOH/Na_2SiO_3$ (%*v*/*v*)
				Na/Si	Si/Al	
WB-N6	100/0	6.0	2.8	0.15	3.12	-
WB-N7	100/0	7.0	3.0	0.17	3.12	-
WB-N8	100/0	8.0	2.8	0.20	3.12	-
WB90-MK10-N7	100/10	7.0	3.0	0.01	2.67	-
WB80-MK20-N7	100/20	7.0	3.0	0.01	2.35	-
WB60-MK40-N7	100/40	7.0	2.5	0.33	1.93	-
WB-SS1-SH1-N7	100/0	7.0	2.8	0.12	3.61	1:1

[1] S/L = solid-to-liquid ratio in the geopolymer paste.

Table 5. Synthesis conditions of potassium-based inorganic polymers.

IP Code Name	WB-2/MK (wt%)	[KOH] (M)	S/L [1] (g/mL)	Molar Ratios		KOH/K_2SiO_3 (%*v*/*v*)
				Na/Si	Si/Al	
WB-K4	100/0	4.0	2.9	0.11	3.12	-
WB-K5	100/0	5.0	2.9	0.12	3.12	-
WB-K6	100/0	6.0	2.9	0.15	3.12	-
WB80-MK20-K5	100/20	5.0	3.0	0.01	2.35	-
WB-PS1-PH1-K5	100/0	5.0	2.9	0.09	3.59	1:1

[1] S/L = solid-to-liquid ratio in the geopolymer paste.

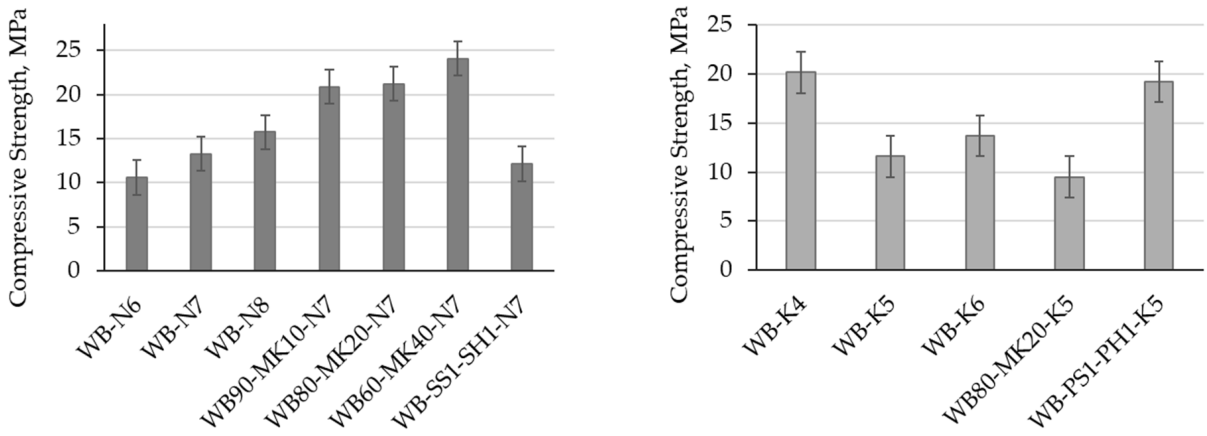

Figure 5. (**a**) Compressive strength of the Na-based inorganic polymers; (**b**) compressive strength of the K-based inorganic polymers. Error bars represent the standard deviation of experimental data. (Experimental conditions: curing at 70 °C for 48 h; hardening for 28 days at ambient temperature).

As shown in Figure 5a, the increase in sodium concentration in the activating solution increased the compressive strength of inorganic polymers, which reached 15.74 MPa for the highest studied sodium concentration of 8 M (mol/L). Moreover, the small addition of metakaolin in the materials synthesis, equal to 10 wt%, dramatically increased their compressive strength by approx. 60% (20.89 MPa). However, further increases in metakaolin content to 20% and 40% resulted in small improvements in compressive strength of about 2% (21.22 MPa) and 15% (24.09 MPa), respectively. Finally, the promotion of the geopolymer system with soluble silicates from the beginning of the geopolymerization process, through the addition of sodium silicate solution, inhibited the development of compressive strength. The increase in soluble silicates in the investigated geopolymer system increased the Si/Al ratio over 3.6 (Table 4). This excess of silicate species, in combination with the low Na/Si ratio, negatively affects the compressive strength of inorganic polymers [27], as it enhances the formation of zeolite phases rather than the geopolymer gel phase [27,28]. In this research work, the Na-based inorganic polymers WB-N8 and WB90-MK10-N7 (Table 4) were considered as optimal and subjected to thermal treatment at elevated temperatures.

According to Figure 5b, the compressive strength of the K-based inorganic polymers studied in this work is optimized at the lowest potassium concentration in the activating solution (4 M), reaching a value of 20.16 MPa. In contrast to the Na-based materials, the addition of metakaolin in the K-based geopolymer system did not improve the compressive strength of inorganic polymers, while the addition of soluble silicates in this system from the beginning of the geopolymerization reaction enhanced their compressive strength. Specifically, the use of an activating solution with potassium silicate and potassium hydroxide solutions in a volume ratio of 1:1 resulted in inorganic polymers with a compressive strength of 19.21 MPa. Based on the experimental results provided in Figure 5b, the K-based inorganic polymers WB-K4 and WB-PS1-PH1-K5 (Table 5) were considered optimal in this research and selected to be exposed to elevated temperatures.

In order to assess the suitability of the optimal Na- and K-based inorganic polymers for TES applications, these materials were exposed to elevated temperatures of 300, 500, and 700 °C. Figure 6 presents their residual compressive strength after exposure to the studied temperatures. The standard deviation of residual compressive strength values is also presented in Figure 6. The density and mass loss of the same materials after their exposure to the studied temperatures are given in Table 6, along with the standard deviation of the reported values. For purposes of comparison, the compressive strength and physical

properties of the inorganic polymers before heating (after curing at 70 °C for 48 h and hardening for 28 days at ambient temperature) are also included in Figure 6 and Table 6 (70 °C).

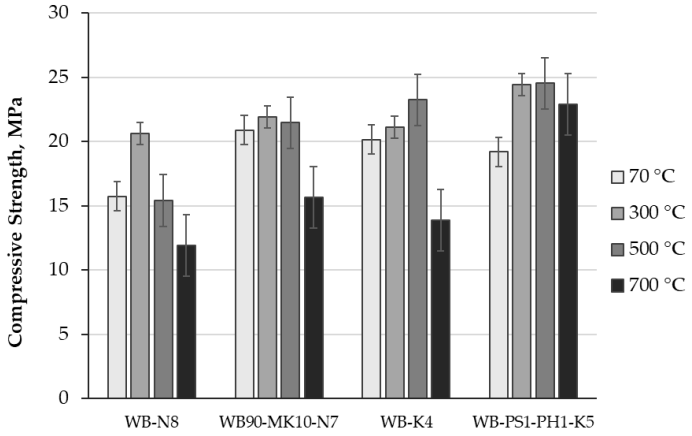

Figure 6. Compressive strength of the optimized Na- and K-based inorganic polymers after curing (70 °C, 48 h) and after exposure to elevated temperatures (300, 500, and 700 °C) for 2 h and cooling down at ambient temperature. Error bars represent the standard deviation of experimental data.

Table 6. Physical properties of optimal inorganic polymers, after exposure to elevated temperatures (in parenthesis, the standard deviation of properties' values is given).

	Density (kg/m^3)				Mass Loss (%)		
	Temperature (°C)						
IP Code Name	**70**	**300**	**500**	**700**	**300**	**500**	**700**
WB-N8	2003 (28.5)	2005 (47.3)	1913 (7.9)	1996 (32.0)	-	20.6 (0.2)	21.6 (0.6)
WB90-MK10-N7	1968 (22.1)	1963 (30.2)	1927 (4.4)	2141 (69.5)	12.6 (1.2)	16.9 (0.4)	26.8 (0.2)
WB-K4	2073 (102.6)	2038 (12.4)	2067 (16.0)	1827 (8.3)	12.5 (0.8)	18.2 (0.5)	12.1 (0.5)
WB-PS1-PH1-K5	2154 (50.8)	2105 (9.6)	2156 (47.0)	2050 (2.3)	9.7 (0.4)	14.0 (0.2)	17.3 (0.5)

According to Figure 6, the residual compressive strength of inorganic polymers was improved with increasing temperature, up to 500 °C. Then, the residual compressive strength of the inorganic polymers was sharply decreased after exposure to 700 °C and went below their initial compressive strength, except for the K-based inorganic polymer that contained the silicate solution (WB-PS1-PH1-K5). This material initially developed very high compressive strength and the highest compressive strength in all the tested temperatures. Especially after exposure to 700 °C, its compressive strength was higher than the initial one. Moreover, the reduction in compressive strength between 500 and 700 °C for this material was only 7%, compared to the relevant reduction in the other inorganic polymers, WB-N8, WB90-MK10-N7, and WB-K4, which was equal to 23%, 27%, and 40%, respectively. After the thermal treatment of the inorganic polymers to 300 °C, no cracks were observed on the sample surface. After treatment at 500 °C, a few surface cracks of small length (<1 cm) were visible, but they were limited to some samples of the inorganic polymers. However, after the exposure of the materials to 700 °C, several intensive cracks were observed in all samples of the sodium-based inorganic polymers. No other signs of spalling, deformation, or damage were visible on these samples. At the temperature of 700 °C, a few cracks were also observed at the K-based inorganic polymers, but they were less pronounced and limited on the sample surface. However, cracks were absent from the K-based samples containing silicate solution. As shown in Figure 6, the cracks that appeared at 700 °C strongly affected the mechanical strength of inorganic polymers.

The observed variations in compressive strength of the inorganic polymers after their exposure to elevated temperatures are related to the mineralogical transformation that occurred in their matrices. In Figures 7 and 8, the XRD patterns of the inorganic polymers WB90-MK10-N7 and WB-PS1-PH1-K5, respectively, after their exposure to the studied elevated temperatures, are illustrated. The XRD pattern of the raw material of the waste bricks (sample WB-1) is also included in Figures 7 and 8 as a control sample [20].

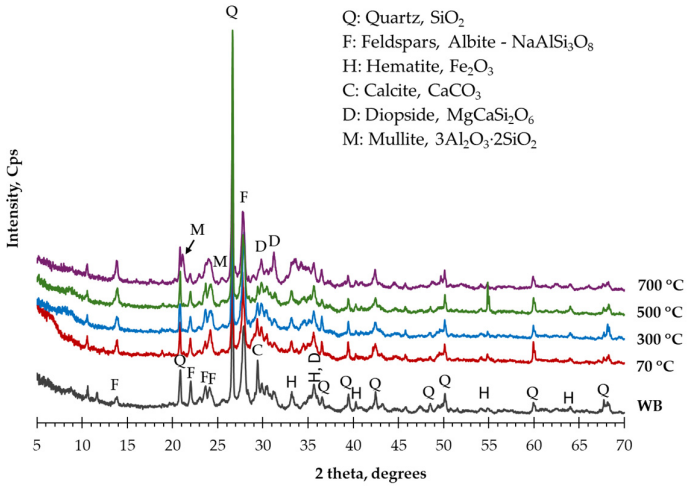

Figure 7. XRD patterns of the raw material WB and the inorganic polymer WB90-MK10-N7, after curing (70 °C/48 h) and 2 h exposure to 300, 500 and 700 °C.

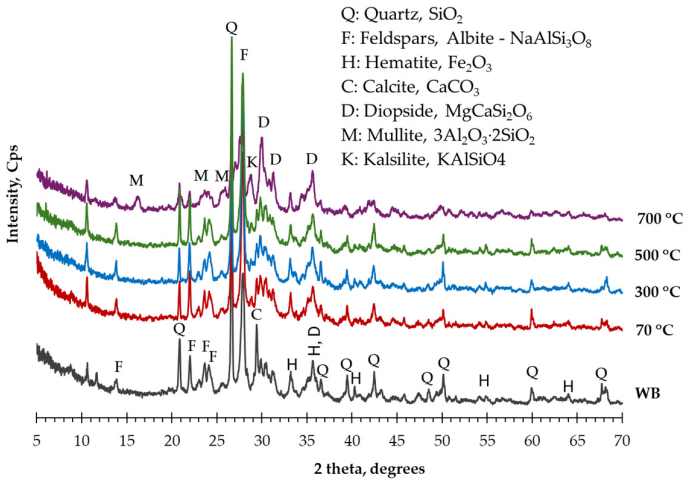

Figure 8. XRD patterns of the raw material WB and the inorganic polymer WB-PS1-PH1-K5, after curing (70 °C/48 h) and 2 h exposure to 300, 500 and 700 °C.

According to Figures 7 and 8, the most important differences observed between the XR patterns of WB and the produced inorganic polymers was the disappearance of calcite in the formed inorganic polymers and the formation of an amorphous phase of aluminosilicate composition, which confirmed the geopolymerization of the WB raw material used in this work. This amorphous phase is identified by the slight broad hump registered in 2theta between 25° and 32° and characterizes the inorganic polymers (geopolymers) [43]. In this work, the formation of the amorphous geopolymer phase indicated partial dissolution of the predominately present feldspars in the produced inorganic polymers. Moreover, it is more intense in the XRD pattern of the inorganic polymer WB-PS1-PH1-K5 (Figure 8) since the corresponding geopolymer system was also provided with soluble silicates (potassium silicate solution) from the beginning of the process. As shown in Figures 7 and 8, no important differences were observed between the initial XRD patterns of the inorganic polymers

WB90-MK10-N7 and WB-PS1-PH1-K5, respectively, and those of the same materials, after their exposure to the temperatures 300 °C and 500 °C. This observation agrees with the almost constant compressive strength of all inorganic polymers to temperatures up to 500 °C (Figure 6). Particularly, in the temperature range from 100 to 300 °C, the removal of the chemically bonded water molecules (dehydration) from the geopolymer matrix takes place [23], while at a slightly raised temperature and up to 350 °C, dehydroxylation of the geopolymer matrix occurs. The low content of water in the inorganic polymers and their micro- to nano-porosity inhibits an intensive expansion, which could lead to cracking and structural damage.

After the exposure of materials to 700 °C, significant mineralogical transformations occurred, as indicated in the relevant XRD patterns. Specifically, the amorphous geopolymer phase identified in the XRD patterns of both inorganic polymers totally disappeared at this temperature due to the melting of this phase and the sintering phenomenon that takes place at temperatures higher than 500 °C [20,23]. Sintering improved the inter-particle bonding in the inorganic polymers, resulting in less porous microstructures, as the geopolymer matrix of materials was densified with the temperature increase [25]. Moreover, the phases of feldspars and hematite, which were detected as predominant in the XRD patterns of both inorganic polymers (Figures 7 and 8), declined importantly in intensity. The phases of diopside and mullite, which were identified in traces in the XRD patterns of both inorganic polymers at temperatures below 500 °C, increased at 500 °C and dominated at 700 °C, along with quartz, as indicated by the increased intensity of the corresponding peaks in the relevant XRD patterns of both materials (Figures 7 and 8). Finally, a newly formed potassium–aluminosilicate phase (kalsilite) was detected in the XRD pattern of the potassium-based inorganic polymer WB-PS1-PH1-K5 (Figure 8). The crystallization of the amorphous geopolymer phase and the mineralogical transformation that occurred after the exposure of the inorganic polymers to 700 °C are associated with the decreasing compressive strength that was observed at this temperature (Figure 6) [20,23,25].

4.2. Thermophysical Properties of Inorganic Polymers at Elevated Temperatures

The thermal conductivity, thermal diffusivity, and heat capacity of a material define its ability to store and transfer heat. These properties are very important for any material that experiences a large or fast temperature gradient, and therefore, they should be considered when selecting or designing TES materials. Table 7 summarizes the thermophysical properties of the inorganic polymers optimized in this research at three different temperatures.

Table 7. Thermophysical properties of optimal inorganic polymers at 100, 300, and 500 °C.

IP Code Name	ρ (kg m^{-3})	Cp (J kg^{-1} °C^{-1})	a × 10^{-7} (m^2 s^{-1})	λ (W m^{-1} °C^{-1})
		100 °C		
WB-N8	2003	924.66	5.2	0.9631
WB90-MK10-N7	1968	956.94	4.7	0.8851
WB-K4	2073	1090.93	5.0	1.1308
WB-PS1-PH1-K5	2154	904.44	5.3	1.0325
		300 °C		
WB-N8	2005	641.81	5.1	0.6563
WB90-MK10-N7	1963	933.79	4.4	0.8065
WB-K4	2038	968.40	4.8	0.9473
WB-PS1-PH1-K5	2105	690.16	5.3	0.7700
		500 °C		
WB-N8	1913	606.91	5.2	0.6037
WB90-MK10-N7	1927	1049.18	4.7	0.9502
WB-K4	2067	903.72	4.8	0.8966
WB-PS1-PH1-K5	2156	729.17	5.6	0.8804

According to Table 7, the thermophysical properties of inorganic polymers showed a small decrease in temperature between 100 and 300 °C, and then they remained almost constant with further increases in temperature to 500 °C. This trend of geopolymers' thermophysical properties to remain relatively constant as temperature increases up to 400–500 °C was also observed in similar research works [33].

The thermophysical properties of the inorganic polymers are similar to those of commonly used sensible heat storage solid-state materials, such as concrete, natural stones, bricks, ceramics, and glass [2], up to 400 °C. The density of different concrete types developed for TES applications ranged from 2203 to 3100 kg m^{-3} [44]. Their heat capacity was in the range of 963 and 1025 J kg^{-1} °C and of 1050 and 1280 J kg^{-1} °C at temperatures of 300 and 400 °C. The same materials presented thermal conductivity between 1.27 and 1.92 W m^{-1} K at 300 °C and between 1.20 and 1.78 at 400 °C [44]. However, their cycle operation was limited to 375 °C for 8 h and to 430 °C for about 1 h. Inorganic polymers remain stable at higher temperatures, exhibiting better properties, which render them significant candidates in thermal energy storage applications. However, further research is needed to investigate their performance and efficiency in such applications.

5. Conclusions

This research revealed that the liquidus temperature surface phase diagrams of the (Na_2O/K_2O)-SiO_2-Al_2O_3 oxide ternary systems, which correspond to the basic geopolymer systems' components, along with the relevant thermodynamic calculations, allow for the theoretical prediction of inorganic polymer (geopolymer) compositions structurally stable at elevated temperatures. Therefore, the thermodynamics of geopolymer systems based on various raw materials comprises an important tool for designing and developing inorganic polymers for thermal energy storage applications.

The most prominent findings of this investigation are the following:

- After optimization, the designed inorganic polymers developed compressive strength close to 20 MPa after curing and hardening, which is comparable to or even higher than that of the solid materials currently used in sensible heat storage applications.
- The addition of soluble silicates and aluminates improved geopolymer systems' compressive strength, in general. The molar ratios of alkali to silicon and silicon to aluminum in the geopolymer system proved important factors affecting the mechanical strength of the final materials.
- After exposure to elevated temperatures up to 500 °C, the compressive strength of all investigated inorganic polymers remained almost constant or was slightly improved. Further increase in temperature reduced the compressive strength, in general.
- The variations in the compressive strength of inorganic polymers observed with the temperature increase were related to the transformations that occurred in the amorphous geopolymer matrix at the relevant temperatures. Specifically, the dehydration and dehydroxylation of this matrix improved the material's durability, while its densification due to the sintering phenomenon enhanced compressive strength. The formation of new crystalline phases and the significant mineralogical alterations occurred in inorganic polymers at 700 °C, which significantly declined their compressive strength.
- Limited surface cracks observed in the inorganic polymers after their exposure to temperatures up to 500 °C did not affect their compressive strength. The intensive cracking of samples observed at 700 °C reduced their compressive strength. No other signs of surface defects, spalling, or deformation were observed after the exposure of the inorganic polymers to all the studied temperatures.
- The thermophysical properties of the optimized inorganic polymers were comparable, or even better, to those currently used in sensible heat storage applications.

– The potassium-based inorganic polymers and the sodium-based one containing a small addition of metakaolin were concluded as the most promising materials for sensible TES.

Author Contributions: Conceptualization, I.G.; methodology, I.G. and K.O.; investigation, K.O., M.S. and L.G.; validation, L.G. and M.S.; visualization, I.G.; writing—original draft preparation, I.G.; writing—review and editing, I.G., A.M. and D.N.; supervision, A.M. and D.N.; project administration, A.M. All authors have read and agreed to the published version of the manuscript.

Funding: This research was co-funded by the Recovery and Resilience Facility of NextGeneration EU Instrument and the Republic of Cyprus under the Grant Agreement No ENTERPRISES/ENERGY/1123/0027.

Data Availability Statement: Data is available upon request.

Acknowledgments: This investigation is performed under the research project entitled "Development of an innovative low-cost and highly efficient energy storage system—DIAS" (ENTERPRISES/ENERGY/1123/0027), which has been co-funded by the Recovery and Resilience facility of the NextGeneration EU Instrument and the Republic of Cyprus. The authors kindly acknowledge also (i) Theodora Kyratsi, Professor at the Department of Mechanical and Manufacturing Engineering of the University of Cyprus for her cooperation in carrying out the mineralogical analysis of geopolymers using the X-ray diffraction method; (ii) Konstantinos Betsis, Junior Researcher at the Laboratory of Metallurgy of School of Mining and Metallurgical Engineering of the National Technical University of Athens for his valuable guidance and contribution to the thermodynamic study and calculations with the FactSage 7.0 software.

Conflicts of Interest: Authors Loizos Georgiou and Alexandros Michaelides were employed by the company RTD TALOS Ltd. The remaining authors declare that the research was conducted in the absence of any commercial or financial relationships that could be construed as a potential conflict of interest.

References

1. The International Energy Agency (IEA). Clean and Efficient Heat for Industry. Available online: https://www.iea.org/commentaries/clean-and-efficient-heat-for-industry (accessed on 27 April 2025).
2. Gunasekara, S.N.; Barreneche, C.; Inés Fernández, A.; Calderón, A.; Ravotti, R.; Ristic, A.; Weinberger, P.; Ömur Paksoy, H.; Koçak, B.; Rathgeber, C.; et al. Thermal Energy Storage Materials (TESMs)—What Does It Take to Make Them Fly? *Crystals* **2021**, *11*, 1276. [CrossRef]
3. Almendros-Ibáñez, J.A.; Fernández-Torrijos, M.; Díaz-Heras, M.; Belmonte, J.F.; Sobrino, C. A review of solar thermal energy storage in beds of particles: Packed and fluidized beds. *Sol. Energy* **2019**, *192*, 193–237. [CrossRef]
4. Alva, G.; Liu, L.; Huang, X.; Fang, G. Thermal Energy Storage Materials and systems for solar energy applications. *Renew. Sustain. Energy Rev.* **2017**, *68*, 693–706. [CrossRef]
5. Koçak, B.; Paksoy, H. Using demolition wastes from urban regeneration as sensible thermal energy storage material. *Int. J. Energy Res.* **2019**, *43*, 6454–6460. [CrossRef]
6. Tripathi, B.M.; Shukla, S.K.; Rathore, P.K.S. A comprehensive review on solar to thermal energy conversion and storage using phase change materials. *J. Energy Storage* **2023**, *72*, 108280. [CrossRef]
7. Raoux, S.; Wuttig, M. Phase Change Materials. *Annu. Rev. Mater. Res.* **2009**, *39*, 25–48. [CrossRef]
8. Punniakodi, B.M.S.; Senthil, R. Recent developments in nano-enhanced phase change materials for solar thermal storage. *Sol. Energy Mater. Sol. Cells* **2022**, *238*, 111629. [CrossRef]
9. Muthukumar, P.; Niyas, H. Materials, Design and Development of Latent Heat Storage Systems for Medium and Large-Scale Applications: Issues and Challenges. In *Encyclopedia of Renewable and Sustainable Materials*, 1st ed.; Hashmi, S., Choudhury, I.A., Eds.; Elsevier: Amsterdam, The Netherlands, 2020; Volume 1, pp. 417–437. [CrossRef]
10. Salgado-Pizarro, R.; Calderon, A.; Svobodova-Sedlackova, A.; Fernandez, A.I.; Barreneche, C. The relevance of thermochemical energy storage in the last two decades: The analysis of research evolution. *J. Energy Storage* **2022**, *51*, 104377. [CrossRef]
11. Felderhoff, M.; Urbanczyk, R.; Peil, S. Thermochemical Heat Storage for High Temperature Applications—A Review. *Green* **2013**, *3*, 113–123. [CrossRef]

12. Barbhuiya, S.; Das, B.B.; Idrees, M. Thermal energy storage in concrete: A comprehensive review on fundamentals, technology and sustainability. *J. Build. Eng.* **2024**, *82*, 108302. [CrossRef]
13. Bergan, P.G.; Greiner, C.J. A New Type of Large Scale Thermal Energy Storage. *Energy Procedia* **2014**, *58*, 152–159. [CrossRef]
14. Laing, D.; Zunft, S. Using concrete and other solid storage media in thermal energy storage (TES) systems. In *Woodhead Publishing Series in Energy, Advances in Thermal Energy Storage Systems*, 1st ed.; Cabeza, L.F., Ed.; Woodhead Publishing: Sawston, UK, 2015; pp. 65–86. [CrossRef]
15. Laing, D.; Lehmann, D.; Fib, M.; Bahl, C. Test Results of Concrete Thermal Energy Storage for Parabolic Trough Power Plants. *J. Sol. Energy Eng.* **2009**, *131*, 041007. [CrossRef]
16. Cong, P.; Cheng, Y. Advances in geopolymer materials: A comprehensive review. *J. Traffic. Transp. Eng.* **2021**, *8*, 283–314. [CrossRef]
17. Castillo, H.; Collado, H.; Droguett, T.; Vesely, M.; Garrido, P.; Palma, S. State of the art of geopolymers: A review. *e-Polymers* **2022**, *22*, 108–124. [CrossRef]
18. Arioz, O. Effects of elevated temperatures on properties of concrete. *Fire Saf. J.* **2007**, *42*, 516–522. [CrossRef]
19. Lahoti, M.; Tan, K.H.; Yang, E.H. A critical review of geopolymer properties for structural fire resistance applications. *Constr. Build. Mater.* **2019**, *221*, 514–526. [CrossRef]
20. Giannopoulou, I.; Robert, P.; Sakkas, K.; Petrou, M.; Nicolaides, D. High temperature performance of geopolymers based on construction and demolition waste. *J. Build. Eng.* **2023**, *72*, 106575. [CrossRef]
21. Martin, A.; Pastor, J.Y.; Palomo, A.; Fernández Jiménez, A. Mechanical behaviour at high temperature of alkali-activated aluminosilicates (geopolymers). *Constr. Build. Mater.* **2015**, *93*, 1188–1196. [CrossRef]
22. Godinho, D.S.S.; Pelisser, F.; Bernardin, A.M. High temperature performance of geopolymers as a function of the Si/Al ratio and alkaline media. *Mater. Lett.* **2022**, *311*, 131625. [CrossRef]
23. Liu, Y.; Hu, X.; Du, Y.; Nematollahi, B.; Shi, C. A review on high-temperature resistance of geopolymer concrete. *J. Build. Eng.* **2024**, *98*, 111241. [CrossRef]
24. Rihan, M.A.M.; Onchiri, R.O.; Gathimba, N.; Sabuni, B. Effect of elevated temperature on the mechanical properties of geopolymer concrete: A critical review. *Discov. Civ. Eng.* **2024**, *1*, 24. [CrossRef]
25. Nassar, R.D.; Zaid, O.; Althoey, F.; Abuhussain, M.A.; Alashker, Y. Spalling behavior and performance of ultra-high-performance concrete subjected to elevated temperature: A review. *Constr. Build. Mater.* **2024**, *411*, 134489. [CrossRef]
26. Barzoki, P.K.; Gowayed, Y. Tailoring metakaolin-based geopolymers for high-temperature stability: Chemical, thermal & mechanical insights. *Ceram. Int.* **2025**, *51*, 11346–11353. [CrossRef]
27. Giannopoulou, I.; Nicolaides, D. Inorganic Polymers (Geopolymers) Based on Construction and Demolition Waste for Fire Safety of Buildings and Constructions. In *Fire Safety Engineering—Measures, Policies, and Applications*; Bedon, C., Ed.; IntechOpen: London, UK, 2025. [CrossRef]
28. Mishra, R.K.; Eren, T.; Wang, D.Y. Inorganic Polymers as Flame-Retardant Materials. In *Smart Inorganic Polymers*; Hey-Hawkins, E., Hissler, M., Eds.; Wiley: Hoboken, NJ, USA, 2019. [CrossRef]
29. Amran, M.; Huang, S.S.; Debbarma, S.; Rashid, R.S.M. Fire resistance of geopolymer concrete: A critical review. *Constr. Build. Mater.* **2022**, *324*, 126722. [CrossRef]
30. Khan, R.; Iqbal, S.; Soliyeva, M.; Ali, A.; Elboughdiri, N. Advanced clay-based geopolymer: Influence of structural and material parameters on its performance and applications. *RSC Adv.* **2025**, *15*, 12443–12471. [CrossRef]
31. Hussain, S.; Amritphale, S.; Matthews, J.; Paul, N.; Matthews, E.; Edwards, R. Advanced Solid Geopolymer Formulations for Refractory Applications. *Materials* **2024**, *17*, 1386. [CrossRef]
32. Bezerra, B.P.; Luz, A.P. Geopolymers: A viable binder option for ultra-low-cement and cement-free refractory castables? *J. Eur. Ceram. Soc.* **2024**, *44*, 5241–5251. [CrossRef]
33. Rahjoo, M.; Goracci, G.; Martauz, P.; Rojas, E.; Dolado, J.S. Geopolymer Concrete Performance Study for High-Temperature Thermal Energy Storage (TES) Applications. *Sustainability* **2022**, *14*, 1937. [CrossRef]
34. Rahjoo, M.; Rojas, E.; Goracci, G.; Gaitero, J.J.; Martauz, P.; Dolado, J.S. A numerical study of geopolymer concrete thermal energy storage: Benchmarking TES module design and optimizing thermal performance. *J. Energy Storage* **2023**, *74*, 109389. [CrossRef]
35. Rahjoo, M.; Goracci, G.; Gaitero, J.J.; Martauz, P.; Rojas, E.; Dolado, J.S. Thermal Energy Storage (TES) Prototype Based on Geopolymer Concrete for High-Temperature Applications. *Materials* **2022**, *15*, 7086. [CrossRef]
36. Frattini, D.; Occhicone, A.; Ferone, C.; Cioffi, R. Fibre-Reinforced Geopolymer Concretes for Sensible Heat Thermal Energy Storage: Simulations and Environmental Impact. *Materials* **2021**, *14*, 414. [CrossRef] [PubMed]
37. Verein Deutscher Eisenhüttenleute (VDEh). *Slag Atlas*, 2nd ed.; Verlag Stahleisen GmbH: Düsseldorf, Germany, 2008; pp. 112+117.
38. De Silva, P.; Sagoe-Crenstil, K. Medium-term phase stability of Na_2O–Al_2O_3–SiO_2–H_2O geopolymer systems. *Cem. Concr. Res.* **2008**, *38*, 870–876. [CrossRef]
39. Trocheza, J.J.; Mejía de Gutiérreza, R.; Riveraa, J.; Bernalb, S.A. Synthesis of geopolymer from spent FCC: Effect of SiO_2/Al_2O_3 and Na_2O/SiO_2 molar ratios. *Mater. Constr.* **2015**, *65*, e046. [CrossRef]

40. Juengsuwattananon, K.; Winnefeld, F.; Chindaprasirt, P.; Pimraksa, K. Correlation between initial SiO_2/Al_2O_3, Na_2O/Al_2O_3, Na_2O/SiO_2 and H_2O/Na_2O ratios on phase and microstructure of reaction products of metakaolin-rice husk ash geopolymer. *Constr. Build. Mater.* **2019**, *226*, 406–417. [CrossRef]
41. Verma, N.K.; Rao, M.C.; Kumar, S. Effect of Curing Regime on Compressive Strength of Geopolymer Concrete. *IOP Conf. Ser. Earth Environ. Sci.* **2022**, *982*, 012031. [CrossRef]
42. Castillo, H.; Collado, H.; Droguett, T.; Sánchez, S.; Vesely, M.; Garrido, P.; Palma, S. Factors Affecting the Compressive Strength of Geopolymers: A Review. *Minerals* **2021**, *11*, 1317. [CrossRef]
43. Panias, D.; Giannopoulou, I.; Perraki, T. Effect of synthesis parameters on the mechanical properties of fly ash-based geopolymers. *Colloids Surf. A Physicochem. Eng. Asp.* **2007**, *301*, 246–254. [CrossRef]
44. Wang, S.; Abdulridha, A.; Bravo, J.; Naito, C.; Quiel, S.; Suleiman, M.; Romero, C.; Neti, S.; Oztekin, A. Thermal energy storage in concrete: Review, testing, and simulation of thermal properties at relevant ranges of elevated temperature. *Cem. Concr. Res.* **2023**, *166*, 107096. [CrossRef]